

FusWay: Multimodal hybrid fusion approach. Application to Railway Defect Detection

Alexey Zhukov

University Bordeaux, CNRS,
Bordeaux INP, INRIA, LaBRI
Talence, France
Ferrocampus
Saintes, France
alexey.zhukov@u-bordeaux.fr

Jenny Benois-Pineau

University Bordeaux, CNRS,
Bordeaux INP, INRIA, LaBRI
Talence, France
jenny.benois-pineau@u-bordeaux.fr

Amira Youssef

SNCF RESEAU, Directions
Techniques Réseau, DGII DTR IP3M
DM Matrice
Paris, France
amira.youssef@reseau.sncf.fr

Akka Zemmari

University Bordeaux, CNRS,
Bordeaux INP, INRIA, LaBRI
Talence, France
akka.zemmari@u-bordeaux.fr

Mohamed Mosbah

University Bordeaux, CNRS,
Bordeaux INP, INRIA, LaBRI
Talence, France
mohamed.mosbah@u-bordeaux.fr

Virginie Taillandier

SNCF, DIR TECHNOLOGIES
INNOVATION ET PROJETS GROUPE,
IR - DPISF TECH4RAIL - TLI
Paris, France
virginie.taillandier@sncf.fr

Abstract

Multimodal fusion is a multimedia technique that has become popular in the wide range of tasks where image information is accompanied by a signal/audio. The latter may not convey highly semantic information, such as speech or music, but some measures such as audio signal recorded by mics in the goal to detect rail structure elements or defects. While classical detection approaches such as You Only Look Once (YOLO) family detectors can be efficiently deployed for defect detection on the image modality, the single modality approaches remain limited. They yield an over-detection in case of the appearance similar to normal structural elements. The paper proposes a new multimodal fusion architecture built on the basis of domain rules with YOLO and Vision transformer backbones. It integrates YOLOv8n for rapid object detection with a Vision Transformer (ViT) to combine feature maps extracted from multiple layers (7, 16, and 19) and synthesised audio representations for two defect classes: rail Rupture and Surface defect. Fusion is performed between audio and image. Experimental evaluation on a real-world railway dataset demonstrates that our multimodal fusion improves precision and overall accuracy by 0.2 points compared to the vision-only approach. Student's unpaired t-test also confirms statistical significance of differences in the mean accuracy.

CCS Concepts

• **Computing methodologies** → **Object detection**; *Feature selection*; • **Applied computing** → Surveillance mechanisms.

Keywords

Multimodal fusion, Hybrid AI, YOLOv8, Vision Transformer, Audio feature synthesis, Railway defect detection application

1 Introduction

The application area of our research is the automatic detection of defects on the rails of railways. Rail networks play an important role in transportation around the world. Defect detection on rail lines is a crucial aspect of ensuring safe and efficient transportation.

The continuous use of rail tracks can lead to various defects, such as cracks, wear, and corrosion. If the defects remain unnoticed and are not regularly inspected, they might pose a significant threat to the safety of passengers and cargo. Therefore, the railway infrastructure is a critical asset that demands continuous monitoring to ensure safety and operational efficiency. With the advent of Artificial Intelligence (AI) the design and implementation of automatic detection systems has become a reality [15]. In such systems, defect detection on rails has transitioned from manual visual analysis by human agents to automated methods, either based on vision systems [9] or employing alternative methods such as ultrasound or electromagnetism [5].

Nevertheless, use of only one modality, e.g. the richest image modality is prone to oversight, especially when subtle defects are present [1]. Vision-based systems—particularly those utilizing convolutional neural networks (CNNs) such as the You Only Look Once (YOLO) family [18, 19] can suffer from high false-positive rates. For example, benign rail joints can be misinterpreted as hazardous defect, leading to unnecessary alarms [13].

Hence it is, particularly important to use all the richness of multimodal information supplied by multi-sensor systems, such as that one presented in [15]. Hence, the adequate multimodal fusion strategies have to be developed for this purpose. Recent research [16] has highlighted the potential of multimodal fusion to overcome single modality limitations by integrating complementary data sources. In particular, audio signals captured during track inspection provide additional context that is often missing from visual data alone [14]. A rail Rupture, for instance, typically produces a distinct, non-repetitive audio impulse, while normal rail joints generate periodic sounds as a train traverses the track.

Transformer architectures have emerged as powerful tools for multimodal fusion, owing to their ability to learn long-range dependencies and align heterogeneous data effectively. Vision Transformers (ViT) have demonstrated promising results in image recognition tasks by leveraging self-attention mechanisms to integrate diverse

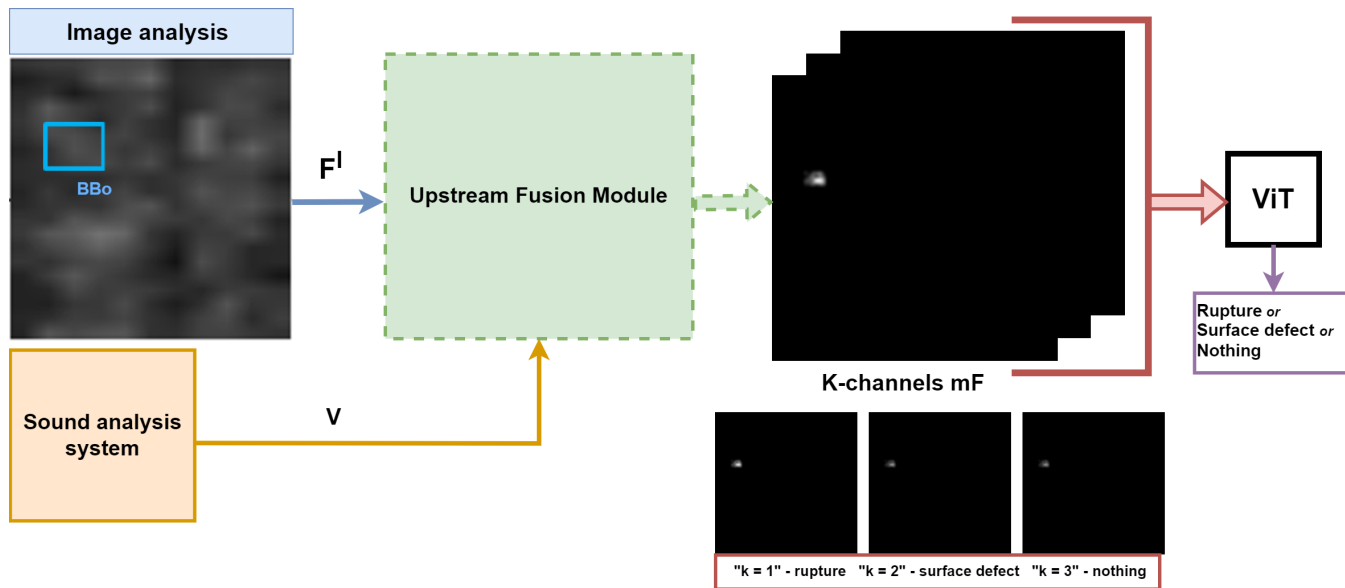


Figure 1: FusWay architecture

features [3]. Extensions of transformer models to multimodal domains further enable the fusion of data, achieving improved performance over unimodal approaches [16, 22]. Such models have been successfully applied in various applications, ranging from sentiment analysis [2] to complex event detection tasks [12].

In this work, we propose a multimodal hybrid AI framework for railway defect detection that fuses visual and synthesised audio features. Our system employs a lightweight YOLO version 8 nano (YOLOv8n) detector to identify candidate defect regions and extract feature maps from multiple layers (7, 16, and 19). These layers capture high-level structural information [7, 8].

Simultaneously, we synthesise audio representations based on established domain knowledge; for example, a rail Rupture is modelled as a singular high-amplitude impulse, while a Surface defect produces a series of irregular, lower-amplitude vibrations [20]. These synthesised audio features are designed to complement the visual data, especially in scenarios where visual ambiguity exists.

To integrate multimodal features both from image and audio modalities, we leverage a Vision Transformer (ViT) [3] as a fusion tool. Furthermore, we propose an upstream fusion module which produces differentiated input to the vision transformer on the basis of class detection probabilities and input measures of the sound and features from YOLOv8n. We note that this methodology is generic and does not depend on the version of YOLO conditionally that convolutional features may be extracted from its layers.

The remainder of the paper is organised as follows. In section 2 we will describe some of the existing multimodal fusion methods in the context of detection on the railway, as well as methods based solely on the image component. In section 3 the method and the architecture of our proposed multimodal fusion model will be presented. In Section 4 we will present our results and analyse them. Finally, Section 5 concludes this work and outlines its perspectives.

2 Related Works

Recent advances in sensor fusion and deep learning have spurred important developments in rail defect detection. The following sections provide an overview of key methodologies and approaches that leverage both multimodal data integration and image-based detection techniques to enhance performance and reliability in this domain.

2.1 Multimodal Fusion

Multimodal fusion in rail defect detection seeks to combine complementary information from different sensor types to overcome the limitations of single-sensor methods.

In [10] a framework is proposed that employs fuzzy logic to integrate features from multiple sensors, such as acoustic, ultrasonic, and vibration data. The authors develop a multi-task detection strategy where the fuzzy inference system models uncertainty and ambiguity inherent in sensor measurements. By considering multiple tasks—such as crack identification, spall detection, and other rail anomalies—the system demonstrates improved precision and robustness compared to traditional threshold-based methods. The fusion of heterogeneous data provides a richer representation of the rail’s condition, thereby enhancing overall diagnostic performance.

In [17] the authors integrate time-series data from vibration sensors with spatial information derived from 2D rail surface images. The approach leverages signal processing techniques to extract meaningful features from 1D vibration signals—such as frequency components indicative of subsurface irregularities—while simultaneously employing convolutional neural networks (CNNs) to capture fine-grained visual details from the images. The fusion is performed at the feature level, allowing the system to benefit from both the temporal dynamics and the high-resolution spatial characteristics. The combined method shows enhanced detection

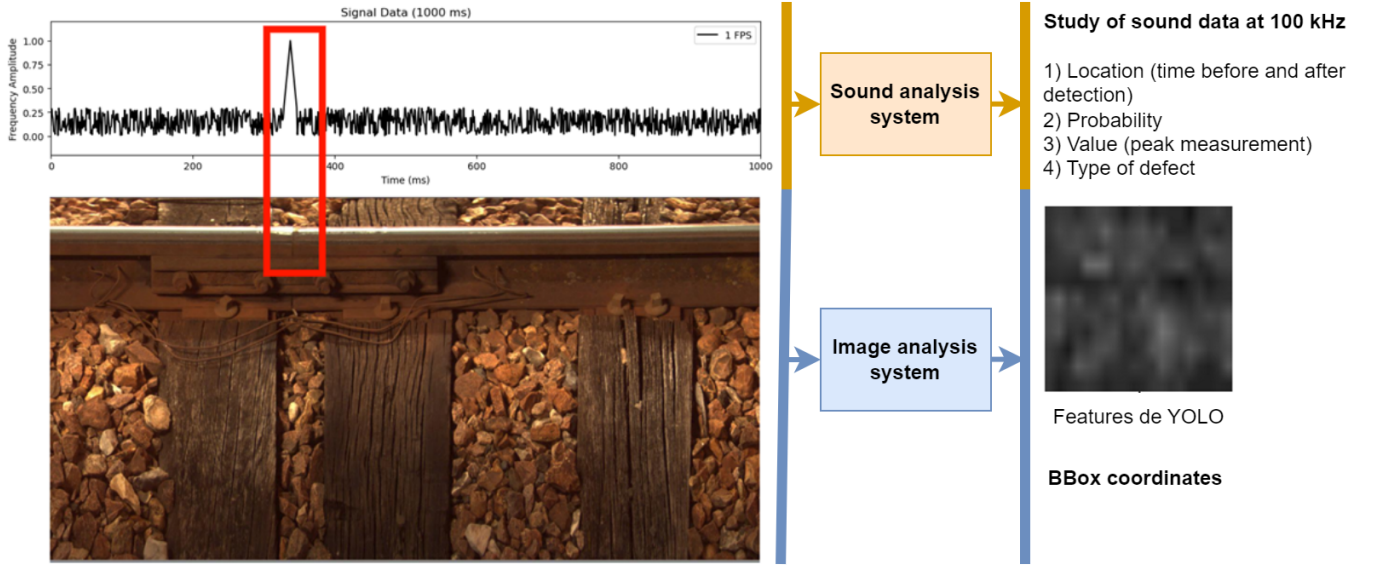


Figure 2: Obtaining characteristics and the result of sound detection

rates, particularly in scenarios where one modality alone may be insufficient due to noise or occlusion.

2.2 Image-Based Detection

Image-based detection has traditionally been a central focus in rail inspection due to the high resolution and detail that visual data can provide.

In [21] a dual-path CNN architecture is introduced which is specifically designed for rail surface inspection. The network consists of two parallel paths: one dedicated to extracting local features that capture small-scale details such as fine cracks or minor spalls, and the other to extracting global contextual features that provide an overall assessment of the rail’s condition. The subsequent fusion of these complementary feature streams allows the system to leverage both detailed texture information and a broader structural context. This architecture is particularly effective in handling challenges such as varying illumination and background clutter, leading to higher detection accuracy and improved resilience under real-world conditions.

The study [22] proposes a hybrid AI framework that combines object-level detection with contextual scene analysis. In this approach, deep learning modules are employed to first localize and classify potential defect regions (object information). Simultaneously, the system analyses the surrounding context—such as rail alignment, track geometry, and environmental factors — to refine and validate the defect detection. By integrating both object and contextual information, the hybrid system can reduce false positives and enhance the reliability of the detection results. This dual-focus strategy is especially beneficial in complex operational settings where isolated visual cues might be ambiguous.

For analysis of visual scenes with the target of specific object (defects) detection, the YOLO family of methods has become extremely popular [8]. This quickly evolving framework allows for

an increased accuracy in defect detection [11]. Nevertheless, without speaking of increased performances of any fusion approach, there are particularities in each application domain which strongly require multimodality. For instance an oil stain on the rail can be confused with a surface defect even by a human operator. Hence, the integration of audio analysis and of other sensors is mandatory.

Therefore, the problem addressed in this research consists in a robust recognition of specific rail defects using image and audio modalities for automatic railway inspection systems. We focus on specific defects: Rail Rupture, Surface defect, and introduce the rejection class “Nothing”.

3 Method

The overall diagram of the proposed method is illustrated in Figure 1. According to the domain knowledge, from left to right three modules are designed: YOLOv8n object detector in the image with sound analysis system, upstream image-audio fusion module (dashed line) and the ViT. We call this module “upstream fusion” as it is introduced before the ViT.

3.1 Overall method

Let us suppose that we have K classes of objects to recognise, amongst which defects, normal structural elements and the rejection class “Nothing”. YOLO detector operates on image modality. We will extract features $F^l \in \mathbb{R}^{K \times W^l \times H^l}$ for the selected layer l from it. The features are then submitted to the upstream fusion module which produces an integrated multi-modal input to the third block, Vision Transformer (ViT) [3]. The upstream fusion block multiplies, element-wise, the features by a tensor $(I^l + V^l)$. Here $I^l \in [1]^{K \times W^l \times H^l}$ is all-ones tensor, $V^l \in \mathbb{R}^{K \times W^l \times H^l}$ with $v_{i,j,k}^l \in [0; 1]$ is the tensor computed from audio features. This yields a tensor of multimodal features $mF^l \in \mathbb{R}^{K \times W^l \times H^l}$. Let us

now consider a mask tensor $M^l \in \mathbb{R}^{K \times W^l \times H^l}$. It masks all the visual features which do not belong to the Bounding Box (BB_O) of an object O detected by YOLO. Formally,

$$m_{i,j,k} = \begin{cases} 1, & \text{if } i, j \in BB_O, \\ 0, & \text{otherwise.} \end{cases} \quad (1)$$

Thus the multimodal masked features submitted by upstream module to the input of the ViT are expressed as in Equation 2

$$mF^l = F^l \otimes (I^l + V^l) \otimes M^l \quad (2)$$

Here \otimes means element-wise multiplication. Note that in our case $K = 3$ as the classes are rail ‘‘Rupture’’, ‘‘Surface defect’’, and ‘‘Nothing’’. The spatial dimensions W^l and H^l depend on the layer of YOLO from where features have been extracted.

The ViT transformer performs the final multi-class classification according to the class taxonomy. Let us now go in deep in extraction of image features F and audio-features V .

3.2 Image Feature Extraction

Image feature tensor $F_0^l \in \mathbb{R}^{C^l \times W^l \times H^l}$ is extracted from the l -th convolutional layer of YOLO object detector with C^l channels. In order to transform the tensor $F_0^l \in \mathbb{R}^{C^l \times W^l \times H^l}$ into the feature tensor $F^l \in \mathbb{R}^{K \times W^l \times H^l}$ for the input of upstream fusion block, an element-wise mean over channel dimension C^l is computed. The feature tensor $F_0^l \in \mathbb{R}^{C^l \times W^l \times H^l}$ is thus squeezed into a feature map of dimension $W^l \times H^l$.

Then the squeezed feature map is normalized to fit $[0, 1]$ and repeated K times to obtain the tensor $F^l \in \mathbb{R}^{K \times W^l \times H^l}$.

3.3 Audio Features Extraction

In the global system of defect detection, audio data are synchronized with image data in the following way. In T seconds of measurement, we obtain N sound amplitude samples. These N measurements are then sent to the audio-analyser. In Figure 2, N corresponds to a sampling rate of 100 kHz and $T = 1$.

Audio features represent an output of audio-analyser. They contain:

- The limits $t_q; t_{q+1}$ of a temporal window where the detection of an event has happened;
- The class probability vector $P_q = (p_1, p_2, \dots, p_k)^T$;
- A normalized measure $G(t) \in [0; 1]$ of the original signal on the temporal window, $t \in [t_q; t_{q+1}]$;
- The most probable class name (type of defect) for detection within the temporal limits $[t_q; t_{q+1}]$.

After obtaining the audio features, we scale the temporal window $[t_q; t_{q+1}]$ relatively to the dimension (height) H^l of image feature tensor F^l we extract from YOLO. Given that the audio system produces N measurements per second while the image feature tensor has a much lower spatial resolution (with height H^l), we map the high-frequency audio data onto the spatial domain via quantization. In this process, the T -second interval corresponding to the whole original image is divided into H^l equal sub-intervals: $\Delta T = \frac{T}{H^l}$ with T in seconds. Thus, each feature row h corresponds to a time interval of duration ΔT . The quantization mapping is defined as: $i = \lfloor \frac{t}{\Delta T} \rfloor + 1$, $t \in [0, T)$,

The temporal interval $[t_q, t_{q+1}]$, corresponding to an event detection, determines the region of interest in the audio data. The set of feature rows corresponding to this interval is given by: $H_q^l = \{i \mid i = \lfloor \frac{t}{\Delta T} \rfloor + 1, t \in [t_q, t_{q+1}]\}$. We have only one measure of audio signal on the interval of detected event: $G(t)_q, t \in [t_q; t_{q+1}]$. Thus, this value is repeated for all feature rows in the region H_q^l . The region H_q^l where the audio analyser computed peak value will be applied to enhance the image features. This peak value $G(t)_q$ is multiplied by the class probability vector P_q to form the weighted peak vector: $GP_q = (G(t)_q \cdot p_1, G(t)_q \cdot p_2, \dots, G(t)_q \cdot p_K)^T$. Then, an all-zeros tensor $[0]^{K \times W^l \times H^l}$ is created, where zeros in the region of the feature row window H_q^l are replaced with the corresponding values from the weighted peak vector GP_q for every ‘‘class’’ layer k . The final tensor V , see Equation 3 thus satisfies:

$$v_{i,j,k} = \begin{cases} (GP_q)_k, & \text{if } i \in H_q^l, \\ 0, & \text{otherwise.} \end{cases} \quad (3)$$

This audio feature tensor is used together with the image feature tensor in the overall upstream fusion block; see Equation 2 to produce the input tensor of the transformer ViT. The latter takes the final decision on the basis of multimodal features. The results of the proposed approach are presented in the following section.

4 Results and discussion

4.1 Dataset

We possess a real-world database of defect and context detection images and an audio database of audio-recordings with microphones mounted on the moving platform. However, due to industrial property rights restrictions, these data cannot be made public, e.g. Open Access. Moreover, audio detections cannot be used directly for security reasons, as they concern tests on railways in Europe. Therefore, after studying the real-world audio dataset, we have synthesised audio features which come from audio detector.

The image dataset consists of images captured in both RGB and grayscale formats at a frame rate of 30 fps by a digital HD camera mounted on the data-recording train’s front wheel. The resolution of images varies from 774×1480 to 1508×1500 . The taxonomy of defects comprises the following classes: ‘‘Rupture, Surface defect, Nothing’’ for rail line defects. The defects elements are annotated with bounding boxes by the experts. The distribution of the quantities of annotated objects per class is given in Table 1. We refer the reader to [23] for a detailed description of the corpus. In the present research we focus on the defects as rail ‘‘Rupture’’ and ‘‘Surface defect’’. It should be mentioned that, due to the extreme rarity of ‘‘Rupture’’, instead for image and audio we used a technically similar element, Seal. Both elements are described as rail breaks characterized by the presence of a more or less pronounced discontinuity in the running surface. Unlike the true ‘‘Rupture’’, the Seal is a periodically detectable element that possesses contextual surroundings. Thus, it might allow for differentiation [22]. In the audio modality, it is represented by an ascending sequence of values up to a certain peak, followed by a subsequent decline. The upstream audio detectors’ outputs are thus modelled by a signal with peaks and noise, as illustrated in Figure 2. To synthesize our audio features, we did not rely on GANs [6], as the amount of real-world detected ‘‘Rupture’’s

Table 1: The total number of examples provided for defects.

Class	#Ex Train	#Ex Val	#Ex Total
Rupture	6441	1715	8156
Surface defect	2679	347	3026
Nothing	9617	1373	10990
Total	18737	3435	22172

and ‘‘Surface defect’’s is relatively small - some dozens. Instead, we applied classical methods of random generation on already normalized audio data, generating both the probability of defects and the normalized audio feature value. The random peak value $Rp_i(e)$ for a class e from our three class taxonomy, is calculated with Uniform Distribution (U) using the formula:

$$Rp_i(e) = a(e) + (b(e) - a(e)) \cdot u_i, \quad (4)$$

$$u_i \sim U(e), \quad i \in \{0, 1, \dots, N - 1\}$$

Here N is the number of detections. The following intervals (a, b) for the peak values were fixed based on the analysis of real-world data. For ‘‘Nothing’’ class: (0, 0.2), ‘‘Surface defect’’: (0.3, 0.6), ‘‘Rupture’’: (0.8, 1). For probabilities generation, the probability of the chosen class (e) is computed using: $p_e = U(0.7, 1)$. The next class probability will be generated in the remaining interval: $p_{e+1} = U(0, 1 - p_e)$. The last class probability will be the rest: $p_{e+K-1} = 1 - p_e - \dots - p_{e+K-2}$. In the context of our multimodal task, defects such as Defective fastener and Missing nut are interpreted as ‘‘Nothing’’ because they do not exhibit audio data distinct from ambient noise. The number of annotated defects, i.e. objects of interest, is 18737. An example of the data is presented in Figure 2.

4.2 Performance Evaluation Methodology

Our three stage architecture is designed in the goal to confirm or filter out false classifications on a single image modality performed by YOLO. The ViT is the final decision component which realises this task by a multi-class classification. For the efficiency analysis, in our experiments we first compute per-class metrics Precision, Recall, F1, Acc, and TNR using one-against-all scenario. They are then combined for the overall system assessment.

One-against-all evaluation. A single target category (e.g., ‘‘Rupture’’) is considered, while all other classes are grouped into the ‘other’ (‘‘non-Rupture’’ respectively) category. The definitions of True Positives (TP), True Negatives (TN), False Positives (FP) and False Negatives (FN) are presented below.

- (1) **YOLO TP.** A generated bounding box (bbox) is considered a true positive if it meets the Intersection over Union (IoU) threshold with the Ground Truth (GT) box belonging to the target category and its classification matches the target category.
- (2) **YOLO FP.** A bounding box is determined as a false positive if the model classifies it as belonging to the target category but it does not meet the IoU threshold with the GT box of the target category, or if it corresponds to a GT box belonging to another category (i.e., it is incorrectly interpreted as an object of the target category).
- (3) **YOLO FN.** This occurs when a GT box for a target object exists (i.e., a box that could have been matched with a prediction satisfying the IoU threshold), but YOLO either misclassifies the object as not belonging to the target category or fails to detect it at all.
- (4) **YOLO TN.** The region is correctly identified as not containing a target object. This means either no bounding box is generated, or if a bounding box is present, it does not satisfy the IoU threshold, and the model does not assign it the target category label. This classification will be used in the ablation study, see section 4.5.2. In the following the types of samples classified by the overall multimodal framework are defined. As they result from the last stage of it, - ViT, we will prefix them with ViT. These types will be used in the assessment of the overall multimodal architecture.
- (5) **ViT TP.** This occurs when either YOLO has correctly classified the bounding box (TP), or even if YOLO made an error (FN), ViT correctly identifies the presence of the target category, thereby confirming it as positive.
- (6) **ViT FP.** A situation where YOLO incorrectly predicted a bounding box as positive (FP) or correctly identified it as negative (TN), but ViT assigns it the target category label despite this, incorrectly indicating the presence of the object.
- (7) **ViT FN.** This occurs when YOLO predicted a bounding box that either met the IoU threshold (TP) or was in an uncertain association zone (FN), but ViT classified it as negative—meaning it failed to recognize the target object even though it is actually present.
- (8) **ViT TN.** A situation where YOLO correctly predicted the absence of a target object (either FP or TN), and ViT confirms this result by not assigning it the target category label, correctly determining that the target object is absent from the image.

Furthermore, we will also compute global metrics such as Accuracy, Recall, Precision, F1, TNR for the overall multi-class classification problem.

4.3 Choice of optimal Feature Layer from YOLO

According to our fusion scheme, image modality features have to be extracted from YOLO detector. This extraction can be performed from different convolutional layers. We try to find a good balance between the feature expressiveness, their richness, and the computation burden for upstream fusion. Hence, we have tested three layers of YOLOv8n convolutional features (7, 16, 19) which have been extracted after the nonlinear layer (Sigmoid-Weighted Linear Unit (SiLU) function [4]). These layers produce tensors of features with different dimensions (w, h, d): $X \in \mathbb{R}^{w \times h \times d}$. The feature vectors of the layer 7 are of (20, 20, 128) dimension, at the layer 16, they are of (40, 40, 64), and at the layer 19 they are of dimension (20, 20, 128). The prevalent criterion of the selection was the final accuracy of the overall system. We discovered that the effectiveness of the Visual Transformer does not depend on the selection of YOLO layer to obtain the features. With each of the three layers and default IoU (30%) for comparison of GT BB and BB predicted by YOLO, the

Table 2: Performance evaluation for YOLOv8n+ViT (layer 7) across three classes

Class	Rupture			Surface Defect			Nothing		
IoU	0.7	0.5	0.3	0.7	0.5	0.3	0.7	0.5	0.3
TP	547	646	684	85	112	118	655	691	699
FP	249	150	113	72	48	48	492	457	455
FN	270	171	133	90	63	57	66	30	22
TN	39	36	31	29	27	26	63	49	29
P	0.6872	0.8116	0.8582	0.5414	0.7000	0.7108	0.5711	0.6019	0.6057
R	0.6695	0.7907	0.8372	0.4857	0.6400	0.6743	0.9085	0.9584	0.9695
F1	0.6782	0.8010	0.8476	0.5120	0.6687	0.6921	0.7013	0.7394	0.7456
ACC	0.5303	0.6800	0.7440	0.4130	0.5560	0.5783	0.5627	0.6031	0.6041
TNR	0.1354	0.1935	0.2153	0.2871	0.3600	0.3514	0.1135	0.0968	0.0599

Table 3: Performance evaluation for YOLOv8n (layer 7) across three classes

Class	Rupture			Surface Defect			Nothing		
IoU	0.7	0.5	0.3	0.7	0.5	0.3	0.7	0.5	0.3
TP	314	587	679	67	110	118	606	684	699
FP	482	209	118	90	50	48	541	464	455
FN	503	230	138	108	65	57	115	37	22
TN	39	34	32	28	26	26	93	25	12
P	0.3945	0.7374	0.8519	0.4268	0.6875	0.7108	0.5283	0.5958	0.6057
R	0.3843	0.7185	0.8311	0.3829	0.6286	0.6743	0.8405	0.9487	0.9695
F1	0.3893	0.7278	0.8414	0.4036	0.6567	0.6921	0.6488	0.7319	0.7456
ACC	0.2638	0.5858	0.7353	0.3242	0.5418	0.5783	0.5159	0.5860	0.5985
TNR	0.0749	0.1399	0.2133	0.2373	0.3421	0.3514	0.1467	0.0511	0.0257

final accuracy of our system was 0.6445. Hence we have chosen the layer 7, which is the last layer of backbone in YOLOv8n, it also has the smallest spatial dimensions of 20×20 . In the following we present the results of our system with these image features only.

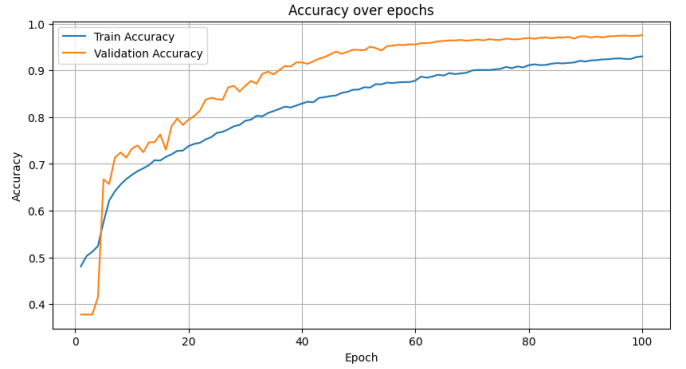
4.4 Fusion with Visual transformer

Table 4: Number of images used to train, to validate and to test visual transformer model.

Stage	#For Train	#For Val	#For Test
Rupture	6441	898	817
Surface defect	2679	172	175
Nothing	9619	650	721

The visual transformer has as input the tensor of multimodal class features coming from upstream fusion Module, see Figure 1 and section 3. The resolution of it is quite low, $w = 20, h = 20, d = 3$. Hence, we used the parametrization of window size for token building as 20% of the spatial dimension of the feature tensor $w \times h$, namely 4×4 in our case. The number of heads was also reduced as the input is of low dimension and contains less details than original images. The number of heads was thus 4.

The transformer was trained on the features extracted from training set of YOLO, using the same validation dataset, as presented in the table 1, with ADAM method as in [3], fixed learning rate

**Figure 3: Training accuracy curves of ViT for the feature maps obtained from 7th layer of YOLOv8n detector.**

of 10^{-6} and early stopping at 100 epochs. The graphs of train and validation accuracy are shown in Figure 3. They are close and exhibit stable behaviour around 100th epoch.

4.5 Results and Ablation study

In this section we will first present the results of our overall scheme and then the ablation study we have performed.

4.5.1 Results of the overall FusWay. Several parameters influence the results of the overall fusion scheme, the first of them is the

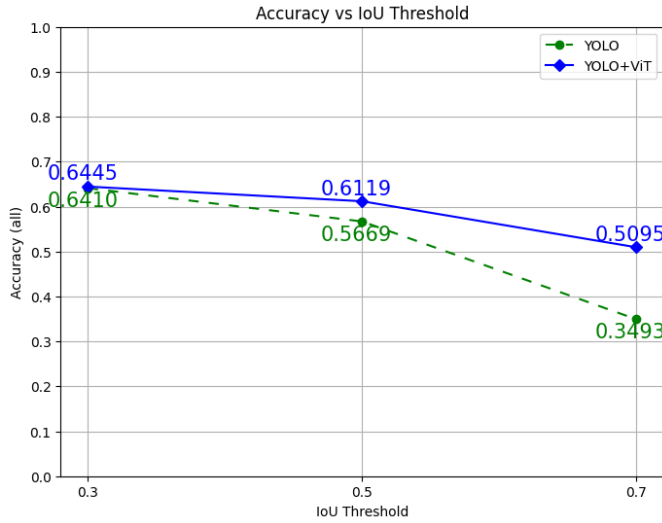


Figure 4: Accuracy change depending on IoU for YOLOv8n and for YOLOv8n+ViT.

YOLO IoU for the given class probability threshold. A bounding box is considered as TP if the IoU with the ground truth BB of an object is higher than a given threshold. The grid search was performed on several threshold values using the default probability threshold $Th_p = 0.25$ from [3]. The overall accuracy plot as a function of threshold is presented in Figure 4. The lower curve corresponds to the accuracy on the image modality only and the higher curve, to the overall FusWay scheme. The difference varies from 0.004 for the most permissive IoU of 0.3 up to 0.16 for the most strict IoU of YOLO. Hence, we can conclude that the adding of hybrid - detection/value audio features and fusion with the transformer allows for improving global accuracy, when the precision of localization of the objects (defects) is important. The results of the overall scheme for the three classes we focus on, are presented in Table 5. Indeed, the fusion with audio features improves the overall accuracy for all IoU values. The improvement in all TP, FP, TN, FN numbers is observed with the most permissive IoU of YOLO. Nevertheless, if the most strict (0.7) IoU is applied, then the number of TP increases by 30% (1287 vs 987), the number of FP decreases by 27%, the number of FN decreases by 41% while the number of TN decreases by 18%, which is not important when the application requires over-detection better than miss-detection. As per-class accuracy is concerned “Rupture”, “Surface defect” and “Nothing”, the results are presented in the Table 2. The “Rupture” class has the best metrics values compared to the “Surface defect” and “Nothing” class. The explanation of this is that in the case of rail rupture, the audio signal value exhibits a well-pronounced peak and the probability of audio detector is generally strong, which was taken into account in our simulation. Furthermore, when a strict IoU value of 0.7 is parametrised for YOLO detector, the difference in P, R, F1 and ACC metrics with YOLO performing on image modality only is of 0.2 approximately, see first columns of Tables 2 and 3 for comparison. The difference is lower in the case of permissive IoU of 0.3, but still does exist. The data are continuously collected and these figures can move with the

arrival of new recorded defects. “Surface defect” class exhibits the lowest metric values, both in complete FusWay scheme and image modality see columns 3, 6, 9 in Table 2 and in Table 3 respectively. This can be explained by the low representation of this class in the overall recordings and thus less examples for training, see Table 4.

4.5.2 Ablation study. The ablation study in our case consists in detecting the defects only by a well-trained object detector YOLOv8n. In the previous section, we have already discussed the lower performances of the single-image modality scheme such as YOLOv8n, compared to our FusWay.

To confirm the interest of the proposed multimodal scheme, we have conducted statistical tests. Train and validation datasets were randomly split in a Z-fold trial ($Z = 10$). The obtained accuracies a_{I_i} and a_{F_i} , $i = 1, \dots, Z$ of only image modality and complete FusWay scheme were compared with Student’s unpaired t-test. These accuracies are presented in Table 6. The test yielded for IoU = 0.3 a t-statistic = 1.0020 and a p-value = 0.3296, IoU = 0.5 a t-statistic = 10.7040 and a p-value = $3.1036 \cdot 10^{-9}$, for IoU = 0.7 a t-statistic = 42.8514 and a p-value = $1.4261 \cdot 10^{-19}$. Hence, for the permissive IoU, the difference between mean accuracies is not statistically significant. This result is in accordance with the one-fold training (0.6410 and 0.6445 of accuracy respectively, see Figure 4). Since the p-value for tests for more strict IoU (0.5 and 0.7 respectively) is significantly less than the standard level of significance (0.05), we can conclude that the FusWay scheme statistically outperforms the only image modality for more strict IoU, in terms of mean accuracy. Thus, our results show that indeed the FusWay scheme outperforms the single modality scheme.

Table 5: Overall performance evaluation for YOLOv8n and YOLOv8n+ViT (layer 7)

Type	YOLOv8n			YOLOv8n+ViT		
IoU	0.7	0.5	0.3	0.7	0.5	0.3
TP	987	1381	1496	1287	1449	1501
FP	1113	723	621	813	655	616
FN	726	332	217	426	264	212
TN	160	85	70	131	112	86
P	0.4700	0.6564	0.7067	0.6129	0.6887	0.7090
R	0.5762	0.8062	0.8733	0.7513	0.8459	0.8762
F1	0.5177	0.7236	0.7812	0.6751	0.6887	0.7838
ACC	0.3493	0.5669	0.6410	0.5095	0.6119	0.6445

5 Conclusion and perspectives

In this work, we have introduced FusWay, a Multimodal fusion technique for rail defect detection that integrates YOLOv8n detector outputs, synthesised realistic audio features derived from domain knowledge, and intermediate fusion via Vision Transformer. These scheme is hybrid as it integrates an intermediate fusion approach (features), results of event detection from audio signals and the input signal value of detected audio event. Our experiments on a domain-specific dataset have shown that union of audio features with image-based detection leads to an increase in detection accuracy for critical defect with permissive IoU by 0.87% for class “Rupture” and confirmation of accuracy for critical defect class “Surface

Table 6: Accuracy performance evaluation of each split iteration for YOLOv8n and YOLOv8n+ViT (layer 7)

Type	YOLOv8n			YOLOv8n+ViT		
	IoU	0.3	0.5	0.7	0.3	0.5
1	0.6311	0.5737	0.3484	0.6366	0.6135	0.5059
2	0.6229	0.5809	0.3419	0.6269	0.6199	0.5063
3	0.6223	0.5635	0.3453	0.6250	0.6066	0.5004
4	0.6254	0.5668	0.3301	0.6309	0.6115	0.4924
5	0.6362	0.5727	0.3448	0.6390	0.6144	0.5000
6	0.6276	0.5691	0.3450	0.6290	0.6073	0.4986
7	0.6078	0.5479	0.3309	0.6111	0.5882	0.4741
8	0.6339	0.5738	0.3418	0.6381	0.6171	0.4990
9	0.6272	0.5670	0.3394	0.6300	0.6086	0.4912
10	0.6250	0.5650	0.3301	0.6284	0.6110	0.4957
Mean	0.6259	0.5680	0.3398	0.6295	0.6098	0.4964
StD	0.0074	0.0083	0.0066	0.0076	0.0082	0.0088

defect". For restrictive IoU the accuracy increases by 26.65% for class "Rupture" and by 8.88% for class "Surface defect. The modular design of FusWay offers the flexibility to integrate additional primary detectors and sensor modalities. Future iterations of this system could benefit from the incorporation of new detection algorithms and advanced fusion techniques, ensuring adaptability as technological advances emerge. Moreover, the generality of our fusion strategy suggests that similar approaches can be extended to other object detection tasks beyond rail defect detection, where combining complementary information from different sources is crucial.

Overall, our technique provides strong evidence that Multimodal fusion AI systems, which leverage both audio and image modalities, hold great promise for solving complex real-world problems. The evolution of such systems will continue to enhance safety and efficiency in rail infrastructure monitoring and other critical applications.

Acknowledgments

This research has been supported by FERROCAMPUS - SNCF - LABRI joint research project under grant agreement AST CT2023-031 under France 2030, EU and Nouvelle-Aquitaine Region.

References

- [1] Ilhan Aydin, Erhan Akin, and Mehmet Karakose. 2021. Defect classification based on deep features for railway tracks in sustainable transportation. *Applied Soft Computing* 111 (2021), 107706.
- [2] Ringki Das and Thoudam Doren Singh. 2023. Multimodal Sentiment Analysis: A Survey of Methods, Trends, and Challenges. *ACM Comput. Surv.* 55, 13s, Article 270 (July 2023), 38 pages. doi:10.1145/3586075
- [3] Alexey Dosovitskiy. 2020. An image is worth 16x16 words: Transformers for image recognition at scale. *arXiv preprint arXiv:2010.11929* (2020). doi:10.48550/arXiv.2010.11929
- [4] Stefan Elfving, Eiji Uchibe, and Kenji Doya. 2018. Sigmoid-weighted linear units for neural network function approximation in reinforcement learning. *Neural networks* 107 (2018), 3–11.
- [5] Wendong Gong, Muhammad Firdaus Akbar, Ghassan Nihad Jawad, Mohamed Fauzi Packer Mohamed, and Mohd Nadhir Ab Wahab. 2022. Nondestructive testing technologies for rail inspection: A review. *Coatings* 12, 11 (2022), 1790.
- [6] Ian Goodfellow, Jean Pouget-Abadie, Mehdi Mirza, Bing Xu, David Warde-Farley, Sherjil Ozair, Aaron Courville, and Yoshua Bengio. 2020. Generative adversarial networks. *Commun. ACM* 63, 11 (2020), 139–144.
- [7] Priyanto Hidayatullah, Nurjannah Syakrani, Muhammad Rizqi Sholahuddin, Trisna Gelar, and Refdinal Tubagus. 2025. YOLOv8 to YOLO11: A Comprehensive Architecture In-depth Comparative Review. doi:10.48550/ARXIV.2501.13400 Version Number: 1.
- [8] Glenn Jocher, Ayush Chaurasia, and Jing Qiu. 2023. *Ultralytics YOLOv8*. <https://github.com/ultralytics/ultralytics>
- [9] Ankit Kumar and S.P. Harsha. 2024. A systematic literature review of defect detection in railways using machine vision-based inspection methods. *International Journal of Transportation Science and Technology* (2024). doi:10.1016/j.ijst.2024.06.006
- [10] Yang Liyuan, Ghazali Osman, Safawi Abdul Rahman, and Muhammad Firdaus Mustapha. 2024. Multi-Modal Fusion for Multi-Task Fuzzy Detection of Rail Anomalies. *IEEE Access* 12 (2024), 73925–73935. doi:10.1109/ACCESS.2024.3397002
- [11] Ming Lu, Wangqi Sheng, Ying Zou, Yating Chen, and Zugu Chen. 2024. WSS-YOLO: An improved industrial defect detection network for steel surface defects. *Measurement* 236 (2024), 115060.
- [12] Rupayan Mallick, Jenny Benois-Pineau, and Akka Zemmari. 2024. IFI: Interpreting for Improving: A Multimodal Transformer with an Interpretability Technique for Recognition of Risk Events. In *MultiMedia Modeling: 30th International Conference, MMM 2024, Amsterdam, The Netherlands, January 29 – February 2, 2024, Proceedings, Part IV* (Amsterdam, The Netherlands). Springer-Verlag, Berlin, Heidelberg, 117–131. doi:10.1007/978-3-031-53302-0_9
- [13] Sasa Radosavljevic, Alain Rivero, Sergio Rodríguez Flórez, Abdelhafid Elouardi, Pauline Michel, Belkacem O Bouamama, and Philippe Vanheeghe. 2024. Performance Evaluation of a Visual Defects Detection System for Railways Monitoring. In *International Conference on Mobility, Artificial Intelligence and Health (MAIH 2024)*, Vol. 69. 03002.
- [14] Md Arifur Rahman, Hossein Taheri, Fadwa Dababneh, Sasan Sattarpanah Kargarroudi, and Seyyedabbas Arhammazi. 2024. A review of distributed acoustic sensing applications for railroad condition monitoring. *Mechanical Systems and Signal Processing* 208 (2024), 110983.
- [15] Alain Rivero, Sasa Radosavljevic, and Philippe Vanheeghe. 2024. Application of Belief Theories for Railway Track Defect Detection. *International Journal of Automation, Artificial Intelligence and Machine Learning* 4, 1 (June 2024), 10–35. doi:10.61797/ijaaiml.v4i1.324 Number: 1.
- [16] Yifei Shen, Qianwen Zhong, Shubin Zheng, Liming Li, and Lele Peng. 2024. A Multi-Modal Approach to Rail Surface Condition Analysis: The MFDF-Net. *IEEE Access* (2024).
- [17] Tiantian Yang, Tianhua Xu, Yu Cheng, Zelong Tang, Shuai Su, and Yuan Cao. 2023. A fusion method based on 1D vibration signals and 2D images for detection of railway surface defects. In *2023 3rd International Conference on Neural Networks, Information and Communication Engineering (NNICE)*. 282–286. doi:10.1109/NNICE58320.2023.10105728
- [18] Chenghai Yu and Zhilong Lu. 2024. YOLO-VSI: An Improved YOLOv8 Model for Detecting Railway Turnouts Defects in Complex Environments. *Computers, Materials & Continua* 81, 2 (2024).
- [19] Danyang Zheng, Liming Li, Shubin Zheng, Xiaodong Chai, Shuguang Zhao, Qianqian Tong, Ji Wang, and Lizheng Guo. 2021. A defect detection method for rail surface and fasteners based on deep convolutional neural network. *Computational intelligence and neuroscience* 2021, 1 (2021), 2565500.
- [20] Shubin Zheng, Qianwen Zhong, Xieqi Chen, Lele Peng, and Guiyan Cui. 2022. The rail surface defects recognition via operating service rail vehicle vibrations. *Machines* 10, 9 (2022), 796.
- [21] Yinfeng Zhong and Guorong Chen. 2024. Rail Surface Defect Detection Based on Dual-Path Feature Fusion. *Electronics* 13, 13 (2024), 2564.
- [22] Alexey Zhukov, Jenny Benois-Pineau, Alain Rivero, Akka Zemmari, Mohamed Mosbah, and Danilo Crispiani. 2024. A Hybrid AI System for Fusion of Object and Context Information: Application to the Rail Line Defect Detection. In *2024 International Conference on Content-Based Multimedia Indexing (CBMI)*. IEEE, 1–7. doi:10.1109/CBIMI62980.2024.10859237
- [23] Alexey Zhukov, Alain Rivero, Jenny Benois-Pineau, Akka Zemmari, and Mohamed Mosbah. 2024. A hybrid system for defect detection on rail lines through the fusion of object and context information. *Sensors* 24, 4 (2024), 1171. doi:10.3390/s24041171